Dielectric function spectra at 40 K and critical-point energies for $CuIn_{0.7}Ga_{0.3}Se_2$

S. G. Choi,[1,a)] R. Chen,[2] C. Persson,[2,3] T. J. Kim,[4] S. Y. Hwang,[4] Y. D. Kim,[4] and L. M. Mansfield[1]

[1]*National Renewable Energy Laboratory, Golden, Colorado 80401, USA*
[2]*Department of Materials Science and Engineering, Royal Institute of Technology, SE-100 44 Stockholm, Sweden*
[3]*Department of Physics, University of Oslo, NO-0316 Oslo, Norway*
[4]*Department of Physics, Kyung Hee University, Seoul 130-701, South Korea*

(Received 20 September 2012; accepted 6 December 2012; published online 26 December 2012)

We report ellipsometrically determined dielectric function ε spectra for $CuIn_{0.7}Ga_{0.3}Se_2$ thin film at 40 and 300 K. The data exhibit numerous spectral features associated with interband critical points (CPs) in the spectral range from 0.74 to 6.43 eV. The second-energy-derivatives of ε further reveal a total of twelve above-bandgap CP features, whose energies are obtained accurately by a standard lineshape analysis. The ε spectra determined by ellipsometry show a good agreement with the results of full-potential linearized augmented plane wave calculations. Probable electronic origins of the CP features observed are discussed. © *2012 American Institute of Physics*.
[http://dx.doi.org/10.1063/1.4773362]

$CuIn_{1-x}Ga_xSe_2$ is so far the most promising thin-film photovoltaic (PV) material and its best cell efficiency has been recorded as high as 20.3%.[1] The production capacity of $CuIn_{1-x}Ga_xSe_2$ solar cells was 426 MW in 2010 and is now approaching gigawatt-scale.[2] For design and optimization of high-efficiency PV device structures, accurate knowledge of the optical response for absorber materials is of great importance.[3] In the course of exploring $CuIn_{1-x}Ga_xSe_2$ for PV device applications, its optical properties were well characterized.[4,5]

Spectroscopic ellipsometry (SE)[6] is known to be a highly suitable method of determining a material's optical functions such as complex dielectric function $\varepsilon = \varepsilon_1 + i\varepsilon_2$ and complex refractive index $N = n + ik$ over a wide spectral range. Therefore, SE has been widely used to characterize various semiconductors.[7] For $CuIn_{1-x}Ga_xSe_2$, SE has been employed to study the composition-dependence of ε and interband critical-point (CP) energies,[8–10] effects of Cu-deficiency on the optical properties,[11] and thin-film growth mechanisms.[12]

The optical information of materials at low temperature, where the thermal broadening of optical transitions is reduced and individual optical structures are better resolved, plays an important role in understanding the material's electronic structure. Hence, the ε spectra for many elemental[13,14] and compound semiconductors[15–17] have been determined by SE at low temperature. However, low-temperature SE study of $CuIn_{1-x}Ga_xSe_2$ is rare despite the availability of rich information on its room-temperature optical properties.

Here, we apply SE to determine the ε spectra of $CuIn_{0.7}Ga_{0.3}Se_2$ at 40 K, a composition for high-performance $CuIn_{1-x}Ga_xSe_2$ PV devices. The SE data are in a good agreement with the ε spectra of $CuIn_{0.5}Ga_{0.5}Se_2$ calculated by the full-potential linearized augmented plane wave (FPLAPW) method using the generalized gradient approximation (GGA) plus an onsite Coulomb interaction U of the Cu d states.[4] The above-bandgap CP energies are obtained from a standard lineshape analysis of SE data. We discuss the probable electronic origins of the observed CP features.

A polycrystalline $CuIn_{0.7}Ga_{0.3}Se_2$ thin film was grown at 600 °C by a single-stage thermal co-evaporation method, where the fluxes of Cu, In, Ga, and Se were kept at constant during the deposition and thus the compositional homogeneity is greatly improved along the growth direction.[18] Ga and In fluxes were maintained at the Ga/(Ga+In) ratio of 0.3, and the atomic Cu ratio Cu/(Ga+In) was approximately 0.87. Soda-lime glass coated with an approximately 1-μm-thick molybdenum (Mo) film was used as the substrate. The nominal thickness of $CuIn_{0.7}Ga_{0.3}Se_2$ thin film was 1.5 μm. Chemical composition of the grown film was determined by X-ray fluorescence.

SE data were collected from 0.74 to 6.43 eV using a dual-rotating-compensators type system (J.A. Woollam Inc., RC-2 model) equipped with a variable-temperature cryostat. The angle of incidence is 68°. We reduced the microscopic roughness of $CuIn_{0.7}Ga_{0.3}Se_2$ film by chemical-mechanical polishing of the surface using a colloidal silica suspension with 0.02-μm particles.

The ε spectra for $CuIn_{0.7}Ga_{0.3}Se_2$ are obtained by the multilayer analysis of the SE data.[19] The multilayer model consists of the ambient, a surface roughness layer, the $CuIn_{0.7}Ga_{0.3}Se_2$ layer, and the Mo layer. The glass substrate is not included in the model because its presence is completely obscured by the metallic Mo layer in the spectral range used for this study. We estimate the surface-roughness layer to be ~2.2 nm thick, and modeled its response as a Bruggeman effective-medium-approximation[20] 50–50 mixture of the $CuIn_{0.7}Ga_{0.3}Se_2$ layer and void. The ε spectra for $CuIn_{0.7}Ga_{0.3}Se_2$ layer were reconstructed by the B-spline formulation.[21]

Real (ε_1) and imaginary (ε_2) parts of the modeled ε spectra for $CuIn_{0.7}Ga_{0.3}Se_2$ taken at 40 and 300 K are given in

a)Author to whom correspondence should be addressed. Electronic mail: sukgeun.choi@nrel.gov.

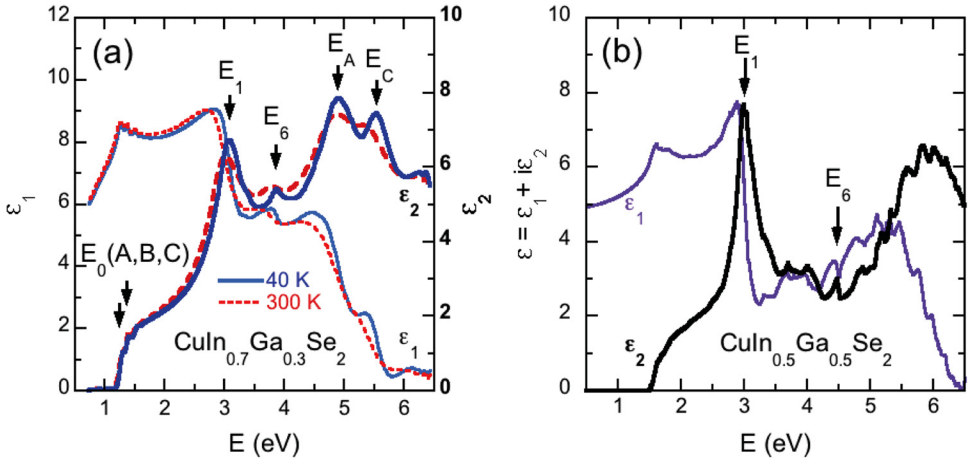

FIG. 1. (a) Modeled ε_1 and ε_2 spectra for $CuIn_{0.7}Ga_{0.3}Se_2$ taken at 40 K (solid blue lines) and 300 K (dashed red lines). Four prominent above-bandgap CP features are indicated by arrows, which are labeled in the numeric and alphabetic order. (b) The ε spectra for $CuIn_{0.5}Ga_{0.5}Se_2$ calculated by the FPLAPW using the GGA + U. The major CP features corresponding to the SE results are identified.

Fig. 1(a). For both temperatures, the optical structures associated with the E_1, E_6, E_A, and E_C interband CPs are clearly seen in the ε_2 spectra at around 3.0, 3.8, 4.8, and 5.5 eV. In the 40 K spectra, however, the CP features are better resolved and their energies increase slightly from those in the 300 K data. For example, the E_C CP feature at ~5.5 eV is seen only as a weak shoulder in the ε_2 spectra at 300 K, but it appears as a distinct peak in the 40 K data. We note that Alonso *et al.*[9] identified the electronic origins of the CP features observed in their room-temperature SE data based on the results from density functional theory calculations done by Jaffe and Zunger.[22] The E_1, E_6, and E_A CPs in our data may correspond to the $E_1(A)$, $E_1(B)$, and $E_2(A)$ CPs in Ref. 9.

The overall shape of the SE-determined ε data shows a good agreement with the averaged $\varepsilon = [2\varepsilon_\perp + \varepsilon_\parallel]/3$ spectrum for $CuIn_{0.5}Ga_{0.5}Se_2$ calculated by the FPLAPW method with the GGA+U potential that is presented in Fig. 1(b). The ordinary ($\varepsilon_\perp$) and extraordinary ($\varepsilon_\parallel$) components of the ε were calculated in our previous work.[4] It appears that the theory slightly underestimates the CP energies below 4 eV, but overestimates those above 4 eV. Although the Ga/(Ga+In) ratio x for the experimental data ($x = 0.3$) and calculated spectrum ($x = 0.5$) are different, our calculations suggest[4] that no significant difference in the optical properties is anticipated between those two close compositions, other than the shift of CP energies. This is also evidenced by the similarities in the calculated ε spectrum and the CP features between $CuIn_{0.5}Ga_{0.5}Se_2$ and $CuInSe_2$.[4]

For the analyses of the observed CP features, we numerically calculated second-energy-derivatives of the *pseudodielectric function*[6] $\langle\varepsilon\rangle$ data using a Savitzky-Golay type[23] linear-filtering algorithm. The CP energies are obtained by assuming the standard analytic CP expressions[24,25] for the lineshapes and then fitting them to the data by least squares schemes. Details of the lineshape analysis procedures can be found elsewhere.[13–16]

The lineshape analysis for the 40 K data is presented in Fig. 2. A total of twelve lineshapes were needed to analyze the data from 2.5 to 6.4 eV. The majority of the CP features are fit best with the two-dimensional lineshapes, whereas the E_2, E_6, E_B CPs are better represented by the excitonic lineshapes and the E_D CP is by the three-dimensional lineshape. Both real and imaginary parts are fit simultaneously. Similar fit quality was achieved for the 300 K data (not shown). The fit-determined CP energies are listed in Table I. For comparison, the CP energies for various $CuIn_{1-x}Ga_xSe_2$ previously reported[8–10,12] are also included. Although Alonso *et al.*[9] observed the E(ΓX) CP at ~2.4 eV for $CuIn_{0.6}Ga_{0.4}Se_2$, our data do not resolve this CP. We note, however, that we probed two additional CPs E_2 and E_4, which have not been seen in previous room-temperature SE studies.[8–10,12]

The electronic origins of each CP are examined based on the results from the FPLAPW calculations. First, we identify the different contributions to ε_2 in terms of the transitions between the valence bands v_i and the conduction bands c_j. Here, the v_1 and c_1 denote the highest valence band and lowest conduction band, respectively. This contribution is labeled as $v_1 \leftrightarrow c_1$ in Fig. 3. As expected,[8,9] the E_0 CPs in the low-energy region are associated with the transitions from v_1 to c_1 near the Γ (0, 0, 0) point of the Brillouin zone (BZ). A broad optical structure in the ε_2 spectrum spanning from 5 to 7 eV is composed of several contributions from the low-lying valence bands. Therefore, unambiguous identification of the major contributions to the CP features in the high-energy region is very difficult.

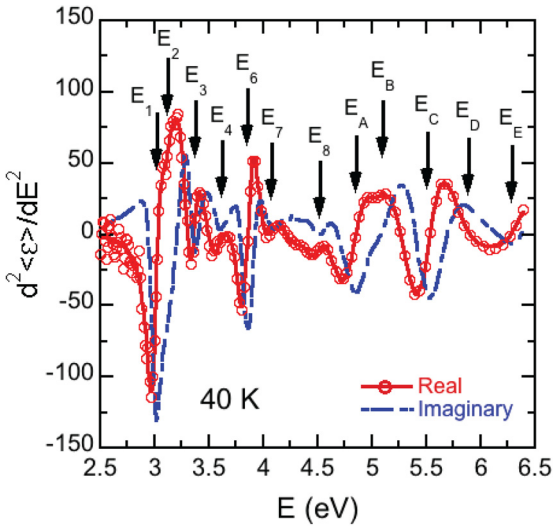

FIG. 2. (a) Solid red are standard CP lineshapes best fit to $d^2\langle\varepsilon_1\rangle/dE^2$ (open circles) and dashed-dotted blue lines are $d^2\langle\varepsilon_2\rangle/dE^2$. For clarity, only half the data points are shown and the $d^2\langle\varepsilon_2\rangle/dE^2$ are not displayed. Energies of each CP are indicated by arrows and labeled in a numeric and alphabetic order.

TABLE I. CP energies in eV for $CuIn_{0.7}Ga_{0.3}Se_2$ at 40 and 300 K. Previously reported CP energies for various $CuIn_{1-x}Ga_xSe_2$ are also included for comparison.

This work $x=0.5$ (Theory)		This work $x=0.3$ (40 K)	This work $x=0.3$ (300 K)	Ref. 12 $x=0.0$ (300 K)	Ref. 8 $x=0.0$ (300 K)	Ref. 8 $x=1.0$ (300 K)	Ref. 9 $x=0.4$ (300 K)	Ref. 10 $x=0.3$ (300 K)
E_0(A,B)	1.48, 1.50	1.33[a]	1.21[a]	1.02	1.040, 1.039	1.648, 1.717	1.22, 1.25	1.168, 1.208
E_0(C)	1.68	1.46[a]	1.44[a]	1.22	1.274	1.92	1.47	1.449
					2.4	2.8	~2.38	
E_1	3	2.998 ± 0.002	2.883 ± 0.015	2.84	2.821/2.901	3.127/3.247	~2.9	2.965
E_2	3.09	3.156 ± 0.006	2.997 ± 0.032					
E_3	3.32	3.342 ± 0.002	3.228 ± 0.003	3.21	3.174	3.501	~3.25	3.302
E_4	3.69	3.548 ± 0.008	3.472 ± 0.001					
E_5	4.02							
E_6	4.47	3.858 ± 0.001	3.755 ± 0.017	3.65	3.635/3.626	4.049/4.03	~3.7	3.746
E_7	4.85	4.192 ± 0.011	4.086 ± 0.185	4.11	4.07	4.49	~4.0	
E_8	5.17	4.504 ± 0.010	4.363 ± 0.062	4.18	4.21		~4.3	
E_A		4.836 ± 0.011	4.760 ± 0.102	4.56	4.71	4.89	~4.7	
E_B		5.120 ± 0.023	5.096 ± 0.374	4.81	4.84	5.1	~5.0	
E_C		5.486 ± 0.008	5.317 ± 0.107	5.11				
E_D		5.857 ± 0.040	5.872 ± 0.086	5.41				
E_E		6.467 ± 0.023	6.419 ± 0.013	5.91				

[a]The E_0(A,B) and E_0(C) energies estimated from the modeled ε_2 spectra.

Second, we analyze the ***k***-dependence of the CPs along the main symmetry directions, which is depicted in Fig. 4. The pronounced E_1 CP originates from the $v_1 \rightarrow c_1$ transitions near the P (1/2, 1/2, 1/2) point of the BZ (in the conventional coordinates). This is consistent with the results from room-temperature SE studies by Alonso *et al.*,[8,9] where this CP is assigned to the E_1(A) CP. We observed a small doublet structure in the E_1 peak arising from the spin-orbit split. The E_2 and E_3 CPs involve transitions from the second valence band, $v_2 \rightarrow c_1$. This band-to-band transition generates two structures in ε_2, where the main peak is associated with transitions at the P-point as for the E_1 CP. In $CuIn_{0.5}Ga_{0.5}Se_2$, the E_2 and E_3 peaks modify only slightly the main ε_2 spectrum around 3.2 eV. However, the calculations for $CuInSe_2$ reveal that the E_2 and E_3 CPs occur 0.1–0.2 eV higher than the E_1 CP, and appear as distinct spectral features. Thus, the observation of E_2 and E_3 CPs in $CuIn_{0.7}Ga_{0.3}Se_2$ is anticipated. The E_4 CP originates from the $v_3 \rightarrow c_1$ transitions at the M (1, 0, 0) = M* (0, 0, 1) point. The E_5 CP is mainly attributed to the transition to $v_4 \rightarrow c_1$ at the N (1/2, 0, 1/2) point, but the $v_3 \rightarrow c_1$ transitions at the M/M* points also contribute to this CP feature. This E_5 CP can be understood as the E_1(B) CP in previous SE studies.[8,9] The E_6 CP feature is a result of the $v_4 \rightarrow c_1$ transition at the N point. The E_7 CP corresponds to the $v_4 \rightarrow c_2$ transitions at the Γ (0, 0, 0) and N point, and the $v_5 \rightarrow c_2$ transitions at the Γ point. The E_A, another prominent CP feature equivalent to the E_2(A) CP in Refs. 8 and 9, also has multiple contributions from the various symmetric points of BZ: The $v_1 \rightarrow c_4$ transitions at the X* (1/2, 1/2, 0) point of the BZ, and the $v_1 \rightarrow c_3$ transitions at the N and P points. We conjecture that the $v_{11} \rightarrow c_1$ and $v_{12} \rightarrow c_1$ transitions near the P point of BZ are the major contributions to the E_C CP. Although this CP has not been discussed in previous SE studies[8,9] of $CuIn_{1-x}Ga_xSe_2$ probably due their limit on the spectral range, a recent real-time SE study[12] of $CuInSe_2$ observed a similar structure at 5.11 eV without identification of its electronic origin.

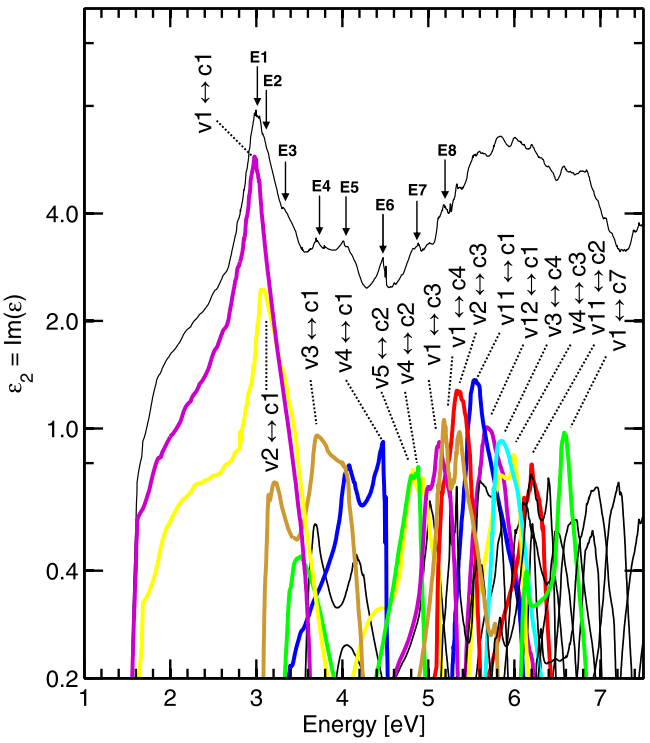

FIG. 3. Band-to-band analysis of the contribution to the total ε_2 spectrum (thin black trace). The most important valence-to-conduction band transitions ($v_i \rightarrow c_j$) are marked by thick colored curves. Spin-orbit interaction is included, and the band-to-band transitions involve a summation of the spin up and down contributions. Note: The vertical axis ε_2 is in the log scale.

Our calculations suggest that the energy differences in the E_0 transitions are E_0(B) − E_0(A) = 0.02 eV and E_0(C) − E_0(A) = 0.20 eV for $CuIn_{0.5}Ga_{0.5}Se_2$, which stem from the negative crystal field split of $\Delta_{cf} = -0.03$ eV and a relatively large spin-orbit split $\Delta_{so} = 0.19$ eV. From the similarities in the valence bands dispersion in $CuIn_{1-x}Ga_xSe_2$ with

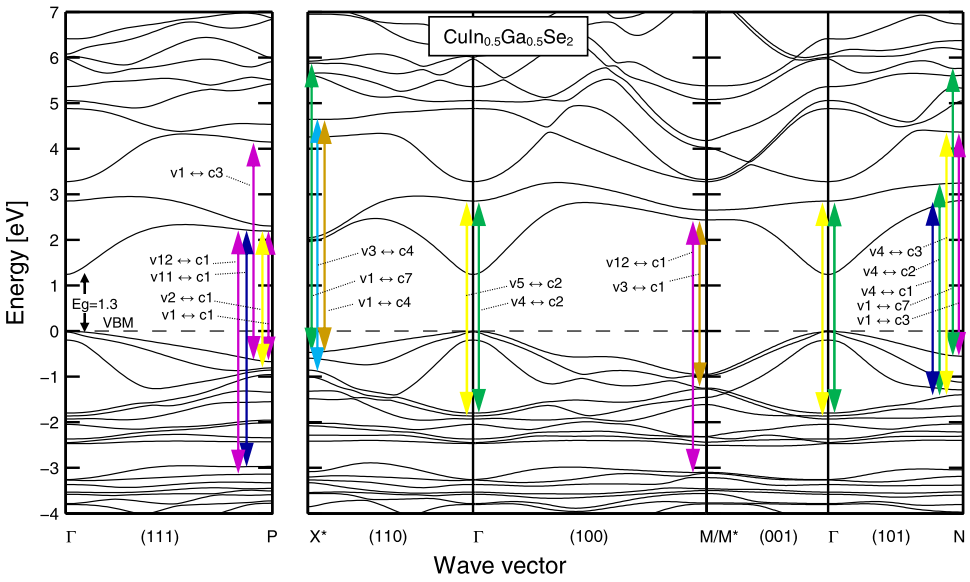

FIG. 4. The calculated electronic band structure of $CuIn_{0.5}Ga_{0.5}Se_2$ where the CPs are identified along the main symmetry directions. Contributions of individual CPs to the ε_2 are shown in Fig. 3.

different alloy compositions,[26] one may expect $\Delta_{cf} \approx 0$ eV and $\Delta_{so} \approx 0.2$ eV for $CuIn_{0.7}Ga_{0.3}Se_2$, which is consistent with our experimental observation.

In summary, the ε spectra for $CuIn_{0.7}Ga_{0.3}Se_2$ were determined by spectroscopic ellipsometry at 40 and 300 K. From a standard lineshape analysis of ellipsometric data, a total of twelve CP energies were obtained from 2.5 to 6.4 eV, which include two additional CPs at 3.01 and 3.48 eV. Electronic origins of the observed CP features were discussed based on the results from FPLAPW calculations of the electronic band structure for $CuIn_{0.5}Ga_{0.5}Se_2$. The pairs of valence and conduction bands along the main symmetry directions of Brillouin zone were suggested for the major CP features observed in the ε_2 spectra.

This work was supported by the U.S. Department of Energy under Contract No. DE-AC36-08-GO28308. The work done at the Royal Institute of Technology was supported by the China Scholarship Council and the Swedish Energy Agency, and with the access to HPC resources at NSC and HPC2N through SNIC/SNAC. The work done at Kyung Hee University was supported by WCU program (Grant No. R33-2011-000-10118-0) and NRF program (Grant No. 2012-0004085) funded by the MEST.

[1]P. Jackson, D. Hariskos, E. Lotter, S. Paetel, R. Wuerz, R. Menner, W. Wischmann, and M. Powalla, Prog. Photovoltaics **19**, 894 (2011).
[2]S. Mehta, PV News **30**, 3 (2011).
[3]O. E. Semonin, J. M. Luther, S. Choi, H.-Y. Chen, J. Gao, A. J. Nozik, and M. C. Beard, Science **334**, 1530 (2011).
[4]C. Persson, Appl. Phys. Lett. **93**, 072106 (2008).
[5]M. J. Romero, H. Du, G. Teeter, Y. Yan, and M. M. Al-Jassim, Phys. Rev. B **84**, 165324 (2011).
[6]D. E. Aspnes, in *Handbook of Optical Constants of Solids*, edited by E. D. Palik (Academic, New York, 1985), chap. 5.
[7]S. Adachi, *Optical Constants of Crystalline and Amorphous Semiconductors: Numerical Data and Graphical Information* (Kluwer Academic, Boston, 1999).
[8]M. I. Alonso, K. Wakita, J. Pascual, M. Garriga, and N. Yamamoto, Phys. Rev. B **63**, 075203 (2001).
[9]M. I. Alonso, M. Garriga, C. A. Durante Rincón, E. Hernández, and M. León, Appl. Phys. A **74**, 6592002
[10]P. D. Paulson, R. W. Birkmire, and W. N. Shafarman, J. Appl. Phys. **94**, 879 (2003).
[11]S.-H. Han, F. S. Hasoon, H. Al. Al-Thani, A. M. Hermann, and D. H. Levi, J. Phys. Chem. Solids **66**, 1895 (2005).
[12]T. Begou, J. D. Walker, D. Attygalle, V. Ranjan, R. W. Collins, and S. Marsillac, Phys. Status Solidi (RRL) **5**, 217 (2011).
[13]L. Viña, S. Logothetidis, and M. Cardona, Phys. Rev. B **30**, 1979 (1984).
[14]P. Lautenschlager, M. Garriga, L. Viña, and M. Cardona, Phys. Rev. B **36**, 4821 (1987).
[15]P. Lautenschlager, M. Garriga, S. Logothetidis, and M. Cardona, Phys. Rev. B **35**, 9174 (1987).
[16]S. Zollner, M. Garriga, J. Humlícek, S. Gopalan, and M. Cardona, Phys. Rev. B **43**, 4349 (1991).
[17]T. J. Kim, J. J. Yoon, S. Y. Hwang, Y. W. Jung, T. H. Ghong, Y. D. Kim, H. Kim, and Y.-C. Chang, Appl. Phys. Lett. **97**, 171912 (2010).
[18]C. L. Perkins, B. Egaas, I. Repins, and B. To, Appl. Surf. Sci. **257**, 878 (2010).
[19]See supplementary material at http://dx.doi.org/10.1063/1.4773362 for detailed information on the sample's microstructure and the multilayer analysis. Modeled refractive index, normal-incidence reflectivity, and penetration depth are also provided.
[20]G. E. Jellison, Jr., L. A. Boatner, D. H. Lowndes, R. A. McKee, and M. Godbole, Appl. Opt. **33**, 6053 (1994).
[21]B. Johs and J. S. Hale, Phys. Status Solidi A **205**, 715 (2008).
[22]J. E. Jaffe and A. Zunger, Phys. Rev. B **28**, 5822 (1983).
[23]A. Savitzky and M. J. E. Golay, Anal. Chem. **36**, 1627 (1964).
[24]M. Cardona, "Modulation spectroscopy," in *Solid State Physics*, edited by F. Seitz, D. Turnbell, and H. Ehrenreich (Academic, New York, 1969), Suppl. 11, p. 119.
[25]D. E. Aspnes, in *Handbook of Semiconductors*, edited by M. Balkanski (North-Holland, Amsterdam, 1980), Vol. 2, p. 109.
[26]R. Chen and C. Persson, Thin Solid Films **519**, 7503 (2011).